

On mechanism of explosive boiling in nanosecond regime

Serap Çelen¹

Received: 1 October 2015 / Accepted: 11 May 2016 / Published online: 1 June 2016
© Springer-Verlag Berlin Heidelberg 2016

Abstract Today laser-based machining is used to manufacture vital parts for biomedical, aviation and aerospace industries. The aim of the paper is to report theoretical, numerical and experimental investigations of explosive boiling under nanosecond pulsed ytterbium fiber laser irradiation. Experiments were performed in an effective peak power density range between 1397 and 1450 MW/cm² on pure titanium specimens. The threshold laser fluence for phase explosion, the pressure and temperature at the target surface and the velocity of the expelled material were reported. A narrow transition zone was realized between the normal vaporization and phase explosion fields. The proof of heterogeneous boiling was given with detailed micrographs. A novel thermal model was proposed for laser-induced splashing at high fluences. Packaging factor and scattering arc radius terms were proposed to state the level of the melt ejection process. Results of the present investigation explain the explosive boiling during high-power laser interaction with metal.

1 Introduction

First mechanism of liquid droplet ejection (LDE) was described by Lord Rayleigh in 1878 [1]. Theoretical investigation of laser-induced liquid droplet ejection (LLDE) during pulsed and q-switched operations was started in 1965 by Ready [2]. In 1972, Dabby and Paek proposed that subsurface heating was the reason of LLDE [3]. In 1976, Von

Allmen [4] reported a comparative investigation about the emission of droplets on copper surface with using Nd:YAG laser pulses. Basu and DebRoy [5] investigated LLDE concept experimentally and theoretically for lead, titanium and stainless steel materials with using carbon dioxide laser pulses which have millisecond pulse durations. In 1987, Chan and Mazumder [6] reported their theoretical analysis for titanium, aluminum and superalloy materials. Aden et al. [7] calculated laser intensity thresholds for aluminum and iron with adopting Euler's equations. In 1995, Miotello and Kelly [8] claimed that the explosive boiling (phase explosion) should be the cause of laser-induced splashing for high laser fluences instead of subsurface heating. Subsurface volume boiling was proposed as the liquid droplet ejection mechanism for silicon surfaces 2 years later [9]. Körner et al. [10] suggested that LLDE was related with material properties and power density levels for nanosecond pulse durations. Lunney and Jordan [11] found that the absorption coefficient was higher than the predicted value and they took attention to the bound-bound and bound-free optical transitions in high density plasma. Spatter deposition area was defined by Low et al. [12] after some drilling experiments of Nimonic 263 alloy with an Nd:YAG laser beam. Willis proposed an approach to describe the behavior of radially distribution of droplets [13].

The importance of explosive phase change on liquid material removal at nanosecond pulsed excimer laser irradiation was reported for nickel material [14, 15]. Solana et al. [16] described two LLDE mechanisms such as melt ejection and radial pressure-based flow. Ghoreishi et al. reported important parameters in Nd:YAG laser-based operations such as the peak power, pulse duration, pulse frequency, number of pulses, assisted gas pressure and focal plane position for stainless steel sheets. Their investigation proved the role of pulse duration and peak power

✉ Serap Çelen
seracelen@hotmail.com; serap.celen@ege.edu.tr

¹ Mechanical Engineering Department, Faculty of Engineering, Ege University, 35100 Izmir, Turkey

Table 1 The laser fluence variation for different investigators

Author [year, reference number]	Laser intensity (MW/cm ²)
Aden [1990, 7]	≤1
Voisey [2003, 19]	0.079–0.087
Von Allmen [1976, 4]	2–100
Low [2000, 12]	2.14
Xu [2000, 14]	100–400
Semak and Matsunawa [1997, 20]	<20
Ready [1965, 2]	1000

on the reproducibility of holes. They showed that the pulse frequency and the number of pulses had not any significant effect for the operation [17]. “Frozen melted droplets” (FMD) phenomenon was first mentioned by Peto et al. [18]. The laser intensity was changed for different investigations [2, 4, 7, 12, 14, 19, 20] (Table 1).

Latest reports were presented in Lasers in Manufacturing Congress [21–24]. Although considerable research has been devoted to establish formulations for surface evaporation, rather, less attention has been paid to report to mathematical model of phase explosion [14, 15, 25–32]. Experimental background emphasized that explosive boiling occurs only if the superheated layer was thick enough; however, there was not any report for its “critical thickness” before the formation of droplet expulsion just after its tearing. Also there is a lack of knowledge for a numerical analysis of droplets (size and morphology) in nanosecond regime for q-switched pulses which have laser intensities upper from 1000 MW/cm². The aim of this present paper is to establish novel mathematical equations to enhance the process quality and reproducibility of laser micro-machining operations. Within the scope of this investigation, a modified Hertz–Knudsen equation was adopted to analyze the liquid–vapor interface after q-switched nanosecond laser irradiation on commercially pure titanium material. A 20 W Telesis (Ohio, USA) ytterbium fiber laser was utilized for experimental tests. The thickness of liquid layer was estimated numerically. Dimensional and morphological data of droplets were given in micrographs. Two additional parameters were defined to enhance process quality such as packaging factor (PF) and scattering arc radius (SAR).

2 Material and method

2.1 Mathematical modeling for laser-induced splashing at high fluences

Kinetic and thermodynamic viewpoints of our approach are shown in Fig. 1. Figure 1a shows the case of normal

vaporization during the laser pulse, 1b, c illustrate after the laser pulse and phase explosion situations, respectively. Gaussian heat source was considered for laser-induced irradiation. The heat flux was calculated by Hertz–Knudsen equation, and it was used to estimate the velocity of surface recession at the liquid–vapor interface (Eq. 1) [33, 34]. The thermal properties of the material were assumed to be constant and thermal expansion was negligible.

$$u_{lpv} \approx \frac{\partial z}{\partial t} \Big|_{z=0} = \frac{\alpha P_s}{\sqrt{(2m_p k_B T_h)}} \left(\frac{m_p}{\rho} \right) \quad (1)$$

Miotello and Kelly reported that the surface temperature was not fixed for laser-induced splashing at high fluences [8]; thus, a modified Clausius–Clapeyron equation was adopted to calculate the saturated vapor pressure [33] (in Eq. 2).

$$u_{lpv} \approx \frac{\alpha P_a}{\sqrt{(2m_p k_B T_h)}} \exp \left[\frac{L_v m_p}{k_B} \left(\frac{1}{T_v} - \frac{1}{T_h} \right) \right] \left(\frac{m_p}{\rho} \right) \quad (2)$$

Two-dimensional Rosenthal equation was used to determine the hot surface temperature (in Eq. 3) [33].

$$\frac{d^2 \phi}{dr^2} + \frac{1}{r} \frac{d\phi}{dr} - \left(\frac{u_{plv}}{2\kappa} \right)^2 \phi = 0 \quad (3)$$

The solution of Eq. 3. was found as a modified Bessel function of the second kind and zero order, and it was given in Eq. 4 [33]. We assumed that the energy flux relocated with the expelled material, and it was equal to the absorbed laser power (q_L), and the power (q_E) which produced in exothermic reaction of titanium with oxygen in the air atmosphere. Process efficiency η_p included the free energy change for nucleation at heterogenous boiling at the transition zone and plasma related energy losses for our novel model. Thus, the heat flux was equal to $\eta_p * (q_L + \eta_E * q_E)$ when r was zero at the center of the laser beam for cylindrical coordinates. Related nomenclature is given in Table 2.

$$T_h = T_0 + \frac{\eta_p * (q_L + \eta_E * q_E)}{2\pi kh} e^{\left(\frac{u_{lpv}^2}{2\kappa} \right)} * K_0 \left(\frac{u_{lpv} r}{2\kappa} \right) \quad (4)$$

The thickness of the liquid layer was estimated with using Eq. 5.

$$\delta_l = (\kappa / u_{lpv}) \text{In}(T_h / T_m) \quad (5)$$

Equation 6 was used to calculate opening area due to laser irradiation.

$$A_e = 2\pi w \delta_l \quad (6)$$

A computer-based calculation program was adopted to calculate the hot surface temperature, the saturated vapor pressure, the velocity of surface recession and the thickness of liquid layer. Related material constants are given in Table 3.

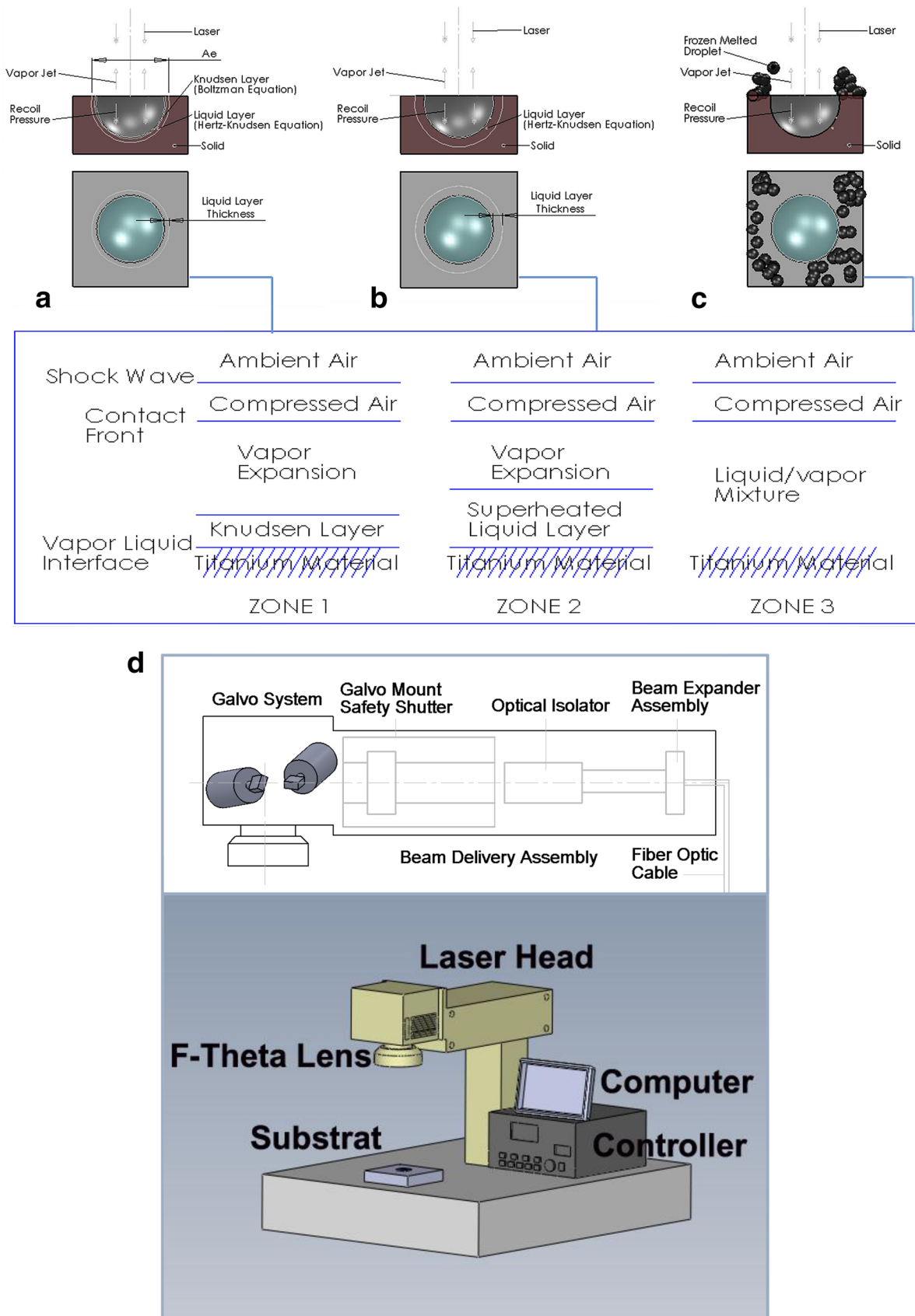


Fig. 1 a–c Schematic representation of laser-induced droplet formation and phase explosion, d schematic representation of laser set-up

Table 2 Nomenclature

Physical properties	Symbol	Unit
Velocity of surface recession	U_{ipv}	m/s
Boltzmann constant	Bt	J/K
Avogadro constant	Na	Mol ⁻¹
Vaporization coefficient	α	–
Saturated vapor pressure	Ps	Pa
Mass of the particle	mp	kg
Ambient gas pressure	Pa	Pa
Vaporization temperature	Tv	K
Hot surface temperature	Th	K
Melting temperature	Tm	K
Ambient temperature	Ta	K
Knudsen layer temperature	Tvk	K
Liquid temperature	Tl	K
Specific heat	Cp	KJ/kg K
Mass density	ρ	kg/m ³
Vaporization enthalpy	L_v	J/kg
Melting enthalpy	Lm	J/kg
Molar mass	M	g/mol
Constant for bessel function	Ko	–
Thickness of the specimen	h	m
Thermal diffusivity	κ	m ² /s
Laser beam radius	w	m
Thickness of liquid layer	δ_l	m
Laser-induced opening area	Ae	m ²
Heat input	ϕ	KJ/m
The distance of any general point	r	m
Laser-induced heat flux (power) input	q_L	Watt
Exothermic reaction-induced heat flux (power) input	q_E	Watt
Efficiency (process)	η_p	–
Efficiency (exothermic reaction)	η_E	–
Plate thickness	h	m
The coordinate point	ξ	–
Melt ejection fraction	MEF	–
Correction factor	C_{xrd}	–
Packaging factor	PF	–
Scattering arc radius	SAR	m

2.2 Quality aspects

Quality of laser micro-machining is related with the narrow heat affected zone, lack of cracking and recast layer, precise geometric dimensions, metallurgical properties and the clean surface finish [33]. In 2003, melt ejection fraction (MEF) term was used to determine the proportion of material removed by laser-induced melt expulsion [19]. (Eq. 7)

Table 3 Calculation parameters

Physical properties	Symbol	Value	Unit
Mass density	ρ	4.51	kg/m ³
Vaporization enthalpy	L_v	8.893×10^6	J/kg
Atomic mass	m	0.47×10^{-26}	kg
Molar mass	M	47.867	g/mol
Laser intensity	I	13.97×10^8 – 14.75×10^8	W/cm ²
Melting temperature	Tm	1941	K
Vaporization temperature	Tv	3533	K
Boltzmann constant	Bt	1.3865×10^{-20}	J/K
Avogadro constant	Na	6.022×10^{23}	Mol ⁻¹
Specific heat	Cp	0.54	KJ/kg.K
Laser beam radius	w	13.35×10^{-6}	m

It was beneficial for drilling applications; however, some manufacturing steps must be involved to obtain clean surface due to splashed particles.

$$MEF = C_{XRD} \frac{\text{Mass gain of collection side}}{\text{Mass loss of drilled sample}} \quad (7)$$

In the present investigation, a packaging factor (PF) and scattering arc radius (SAR) terms were defined to increase the quality of laser-based applications. They can be facilitators for machining blind holes. PF refers the ratio of total accumulated scatterers to a limited surface zone on the target surface. (Eq. 8) If PF has a low value, the scattering is supposed to be low and the process quality will increase. SAR term defines the maximum planar distance of the droplet from the center of the laser-induced opening area. It shows the effect of melt ejection velocity.

$$PF = \frac{\text{Covered zone by accumulated scatterers}}{\text{Limited surface area}} \quad (8)$$

2.3 Experimental configuration

After the required numerical analysis, experiments were conducted to observe the quantity and morphology of frozen melted droplets. ASTM B265 grade 2 commercial pure titanium specimens were molded in acrylic resin. Grinding was carried out under water irrigation using 320, 600, 1200 grit waterproof silicon carbide abrasive papers followed by polishing using 6 μ m and 1 μ m diamond paste on a medium nap rayon cloth. Q-switched mode was used with a galvo steered precise motion control system. (Figure 1d) The wavelength of the laser beam was 1064 nm. With an $f = 160$ mm f-theta lens, a beam waist diameter of 26.7 μ m was obtained with a 90° angle. Pulse repetition rate was adjusted to 10,000 Hz. Specimens were mounted tightly

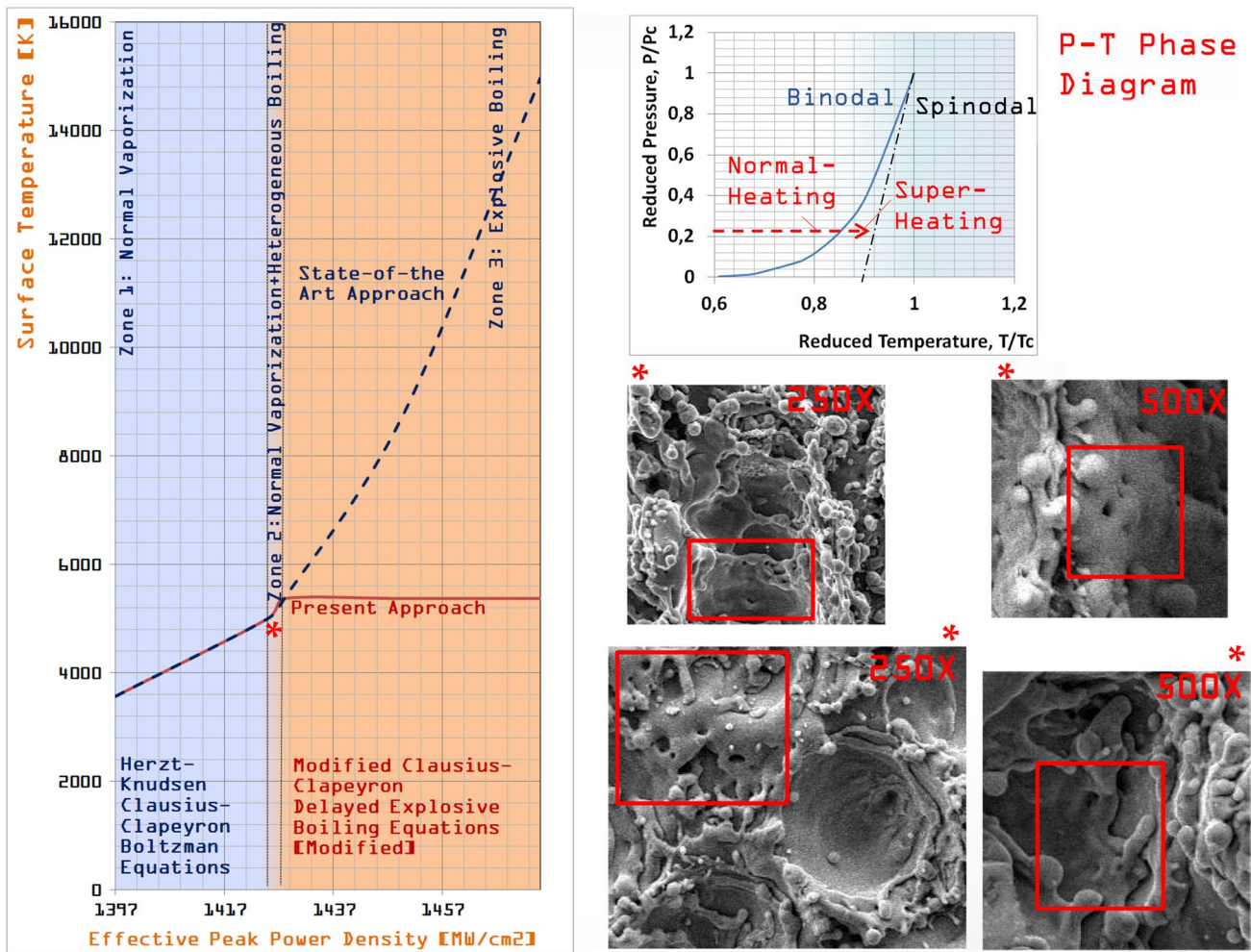


Fig. 2 Graphical representation of the surface temperature and micrographs of heterogeneous boiling

and controlled in order to prevent misplacement. Surfaces of specimens were laser micro-machined by single and double pulses. The main parameters of the laser radiation were as follows: the energy per pulse 1.2–1.8 mJ and the pulse duration 200–250 ns. The maximum effective peak power density value was calculated about 1450 MW/cm².

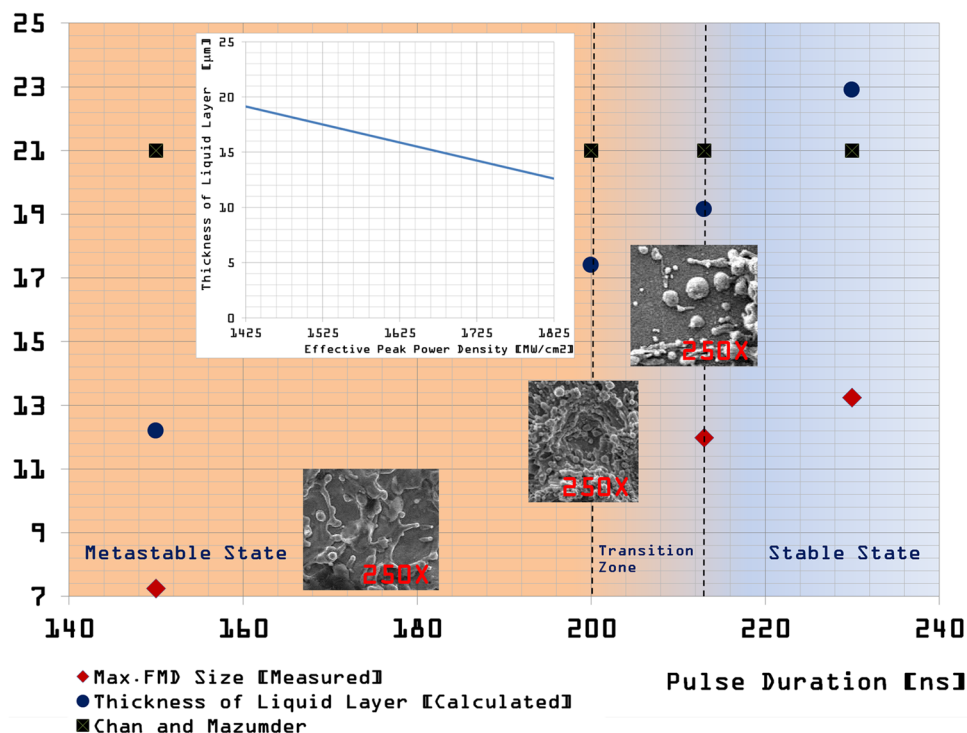
The surfaces of the titanium targets were examined with scanning electron microscope examination (JSM-6060 JEOL).

3 Results and discussion

During q-switched laser irradiation of commercially pure titanium material, the mechanism of liquid metal expulsion has been examined both theoretically and experimentally. According to our numerical analysis, the surface temperature increased with the effective peak power density. Calculated surface temperatures are shown in Fig. 2 for

state-of-the-art [33, 34] and present approaches. Although Knight’s approach was only used for surface evaporation (dot line) [34], our model can be used for both heterogeneous and explosive boiling conditions (straight line). Modified Clausius–Clapeyron model enables vaporization in a temperature range up to critical temperature of titanium instead of a constant value. Thus the surface temperature was not fixed for laser-induced splashing at high fluences [8]. In laser-induced boiling, the surface temperature was supposed to be fixed; however, there should be an increase because of the raising laser power intensity due to heterogeneous vaporization at the same zone. The release of gas from subsurface can be seen in micrographs. When the surface temperature reached to $\sim 0.84 T_c$ ($T_c = 5850$ K-thermodynamic critical temperature of titanium), the saturated vapor pressure was estimated as 4, 64 MPa. The pure titanium material made a rapid transition from superheated liquid to a mixture of liquid droplets and vapor at 5265 K ($\sim 0.9 T_c$). The molten layer was pushed laterally and

Fig. 3 Graphical representation of the maximum droplet size and estimated thickness of the liquid layer, a pearl in the micro-valley 250X



droplets splashed in mostly spherical form to the ablation front. A group of droplets scattered to the outside atmosphere. Some of them accumulated on the specimen surface. Their average velocity was calculated about 0.441 m/s. (with Eq. 1) Chan and Mazumder were reported that the total removal rate of titanium above from 0.4 m/s [6]. Thus, the current algorithm was consistent with the background investigation.

Dimensions of droplets were measured and they compared with estimated thicknesses of liquid layer. The graphical representation of the thickness of liquid layer versus pulse duration is given in Fig. 3. According to the Fig. 3, the maximum droplet size tended to rise with increasing pulse duration. It was observed about 13 μm , and the thickness of the liquid layer was estimated as 22 μm at 230 ns pulse duration. The thickness of the liquid layer was reported about 20 μm for 10 kW laser power [6]. The critical tearing thickness was found about 17 μm . (in Fig. 3 250X zoom-200 ns) At this point, maximum droplet size was measured as 11 μm from scanning electron microscopy micrograph. There was a slight decrease in thickness levels when the effective peak power density increased. (Figure 3 core graph) When the power density increased, the recoil pressure rose and it triggered the vapor to the ablation front [33].

Two process quality factors were proposed. When the packaging factor (PF) proved the dominated mechanism numerically, the scattering arc radius (SAR) showed its level. Total planar surface area of accumulated particles

was measured with using SEM. PF referred the areal proportion of particles on a limited 120 μm^2 surface area. It was multiplied by M factor to cover the lost laser beam area. The change in the quantity of droplets before and after the threshold value can be seen in Fig. 4. Maximum PF was calculated about 70 % for 1.7 mJ heat load. PF increased gradually from 150 to 213 ns pulse durations, and it declined after 213 ns due to the mechanism change at superheated temperature.

Wider liquid layer thickness enabled bigger droplets with lowering their packaging factor value. There was a significant drop in the level of the PF after the threshold. It can be interpreted that the heat rate was so slow and the liquid was not metastable for longer pulse durations [8]. Maximum scattering arc radius (SAR) can be seen in Fig. 4. According to the graph, splashing length rose with increasing pulse duration (with increased recoil pressure and velocity of droplets). The micro-morphology of laser-generated cavity after 1.8 mJ pulse is given in Fig. 4d. Laser-irradiated cavity had contained a little pearl-like frozen melted droplet. This can be called as “sea shell effect.” Our results were appropriate with former studies for pulsed laser operations [12, 20, 35, 36] Although Semak and Matsunawa’s criterion was reported for laser intensities up to 20 MW/cm^2 , its further investigations will be beneficial for high-power regimes [20].

According to the result of the mathematical analysis, significant amount of energy was lost due to the laser-induced plasma. Further SAR investigations will lead to

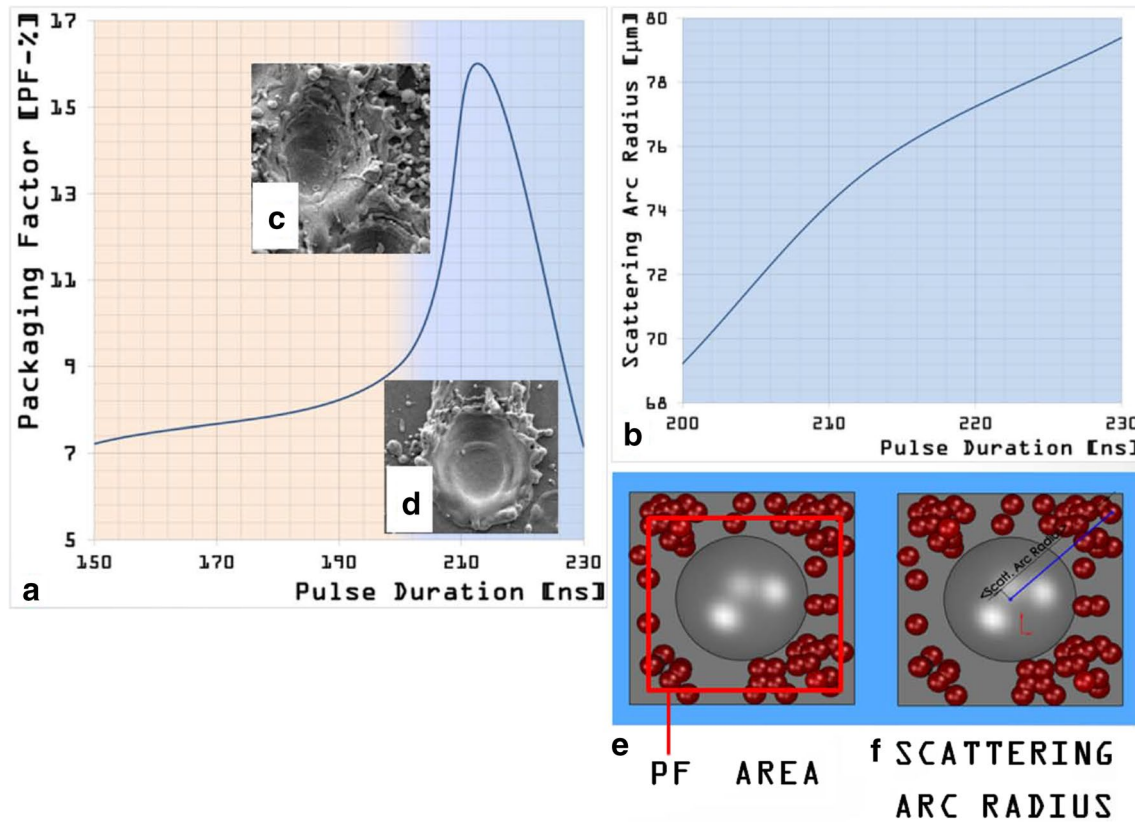


Fig. 4 Graphical representation of **a** packaging factor and **b** scattering arc radius versus pulse duration variation, **c** quantity of frozen melted droplets under the threshold value, **d** quantity of frozen melted droplets upper the threshold value, **e** packaging factor donates the

ratio of total red area to gray zone in a limited red border, **f** scattering arc radius represents the maximum length of droplet to the irradiation cone center

understand Solana's second mechanism about intensity distribution due to the recoil pressure which was not proven until now [16]. Also novel mathematical approaches should be developed to obtain the critical bubble radius (at heterogeneous boiling) and the actual average rate of material removal in the future [37, 38].

4 Conclusion

Our novel model should serve some purposes such as precision control of the laser beam interaction with target. Following conclusions can be summarized in the scope of this investigation;

- This is the first report which explains laser-induced boiling of metals. According to P - V diagram, heterogeneous boiling started at $\sim 0.84 T_c$ -4.64 MPa. The phase explosion was occurred at $\sim 0.9 T_c$ -9.62 MPa.
- The critical thickness of liquid layer was found about 17.4 μm and maximum frozen melted droplet size was measured as 11 μm at this stage. Thicknesses of the

liquid layer were estimated in the range of 12–22 μm for 150–230 ns. The maximum droplet size was changed between 7 and 13 μm for 1.2–1.8 mJ laser intensities, respectively.

- Shapes of droplets were observed mainly spherical form, and the scattering arc radius (SAR) was increased with the pulse duration and pulse energy.
- PF can be used as a numerical parameter to predict vaporization.

Acknowledgments The author would like to thank to ICON Machinery family (<http://www.ikonmakina.com>) for supporting our experimental investigations. Also the author thanks to Prof. Dr. Naoki KISHIMOTO from NIMS/JAPAN, and Dr. Friedrich G. BACHMANN from FRIBA LaserNET/GERMANY and Gulden OZCAN from London/GREAT BRITAIN for their inexhaustible positive energies.

References

- L. Rayleigh, On the Instability of Jets, in *Proceedings London Mathematical Society*, s1-10(1) 4–13 (1878). doi:10.1112/plms/s1-10.1.4

2. J.F. Ready, Effects due to absorption of laser radiation. *J. Appl. Phys.* **36**, 462 (1965). doi:[10.1063/1.1714012](https://doi.org/10.1063/1.1714012)
3. F.W. Dabby, U.C. Paek, High-intensity laser-induced vaporization and explosion of solid material. *IEEE J. Quantum Electron.* **QE-8** (2), 106–111 (1972). doi:[10.1109/JQE.1972.1076937](https://doi.org/10.1109/JQE.1972.1076937)
4. M. Allmen, Laser drilling velocity in metals. *J. Appl. Phys.* **47**, 5460 (1976). doi:[10.1063/1.322578](https://doi.org/10.1063/1.322578)
5. S. Basu, T. DebRoy, Liquid metal expulsion during laser irradiation. *J. Appl. Phys.* **72**, 3317 (1992). doi:[10.1063/1.351452](https://doi.org/10.1063/1.351452)
6. C.L. Chan, J. Mazumder, One-dimensional steady state model for damage by vaporization and liquid expulsion due to laser-material interaction. *J. Appl. Phys.* **62**(11), 4579–4586 (1987). doi:[10.1063/1.339053](https://doi.org/10.1063/1.339053)
7. M. Aden, E. Beyer, G. Herziger, Laser-induced vaporization of metal as a Riemann problem. *J. Phys. D Appl. Phys.* **23**, 655–661 (1990). doi:[10.1088/0022-3727/23/6/004](https://doi.org/10.1088/0022-3727/23/6/004)
8. A. Miotello, R. Kelly, Critical assessment of thermal models for laser sputtering at high fluences. *Appl. Phys. Lett.* **67**(24), 3535–3537 (1995). doi:[10.1063/1.114912](https://doi.org/10.1063/1.114912)
9. V. Craciun, D. Craciun, Evidence for volume boiling during laser ablation of single crystalline targets. *Appl. Surf. Sci.* **138–139**, 218–223 (1999). doi:[10.1016/S0169-4332\(98\)00608-4](https://doi.org/10.1016/S0169-4332(98)00608-4)
10. C. Körner, R. Mayerhofer, C. Hartmann, H.W. Bergman, Physical and material aspects in using visible laser pulses of nanosecond duration. *Appl. Phys. Lett. A* **63**, 288–293 (1996). doi:[10.1007/BF01567639](https://doi.org/10.1007/BF01567639)
11. J.G. Lunney, R. Jordan, Pulsed laser ablation of metals. *Appl. Surf. Sci.* **127–129**, 941–946 (1998). doi:[10.1016/S0169-4332\(97\)00770-8](https://doi.org/10.1016/S0169-4332(97)00770-8)
12. D.K.Y. Low, L. Li, P.J. Byrd, The effect of process parameters on spatter deposition in laser percussion drilling. *Opt. Laser Technol.* **32**(5), 347–354 (2000). doi:[10.1016/S0030-3992\(00\)00079-7](https://doi.org/10.1016/S0030-3992(00)00079-7)
13. D.A. Willis, X. Xu, Transport phenomena and droplet formation during pulsed laser interaction with thin films. *J. Heat Transf.* **122**, 763–770 (2000). doi:[10.1115/1.1288931](https://doi.org/10.1115/1.1288931)
14. X. Xu, K.H. Song, Phase change phenomena during high power laser interaction. *Mater. Sci. Eng.* **A292**, 162–168 (2000). doi:[10.1016/S0921-5093\(00\)00996-5](https://doi.org/10.1016/S0921-5093(00)00996-5)
15. X. Xu, D.A. Willis, Non-equilibrium phase change metal induced by nanosecond pulsed laser irradiation. *J. Heat Transf.* **124**, 293–298 (2002). doi:[10.1115/1.1445792](https://doi.org/10.1115/1.1445792)
16. P. Solana, P. Kapadia, J. Dowden, W.S.O. Rodden, S.S. Kudesia, D.P. Hand, J.D.C. Jones, Time dependent ablation and liquid ejection processes during the laser drilling of metals. *Opt. Commun.* **191**(1–2), 97–112 (2001). doi:[10.1016/S0030-4018\(01\)01072-0](https://doi.org/10.1016/S0030-4018(01)01072-0)
17. M. Ghoreishi, D.K.Y. Low, L. Li, Statistical modelling of laser percussion drilling for hole taper and circularity control. *Proc. Instn. Mech. Eng. Part B J. Eng. Manuf.* (2002). doi:[10.1016/S0890-6955\(02\)00038-X](https://doi.org/10.1016/S0890-6955(02)00038-X)
18. G. Peto, A. Karacs, S. Pastzi, L. Gucci, T. Divinji, A. Joob, Surface treatment of screw shaped titanium dental implants by high intensity laser pulses. *Appl. Surf. Sci.* **186**, 7–13 (2002). doi:[10.1016/S0169-4332\(01\)00769-3](https://doi.org/10.1016/S0169-4332(01)00769-3)
19. K.T. Voisey, S.S. Kudesia, W.S.O. Rodden, D.P. Hand, J.D.C. Jones, T.W. Clyne, Melt ejection during laser drilling of metals. *Mater. Sci. Eng. A* **356**, 414–424 (2003). doi:[10.1016/S0921-5093\(03\)00155-2](https://doi.org/10.1016/S0921-5093(03)00155-2)
20. V. Semak, A. Matsunawa, The role of recoil pressure in energy balance during laser materials processing. *J. Phys. D Appl. Phys.* **30**, 2541–2552 (1997). doi:[10.1088/0022-3727/30/18/008](https://doi.org/10.1088/0022-3727/30/18/008)
21. J.L. Ocana, R. Jagdheesh, J.J. Garcia-Ballesteros, *One-Step Generation of Ultrahydrophobic Aluminum Surface Patterns by Nanosecond Lasers* (Lasers in Manufacturing Congress, Munich, 2015)
22. S. Russ, U. Keller, L. Bauer, T. Meyer, R. Gebbs, B. Faisst, *Shorter than Short: How does the Pulse Duration Influence the Process Efficiency and the Quality of Conductive Materials?* (Lasers in Manufacturing Congress, Munich, 2015)
23. D.J. Förster, V. Onuseit, R. Weber, T. Graf, *Energy Transfer Mechanisms During Laser Pulsed Processing of Metals* (Lasers in Manufacturing Congress, Munich, 2015)
24. M. Sailer, J. Kleiner, M. Kaiser, S. Russ, *Scaling of Ablation Rates. Ablation Efficiency and Quality Aspects of “Burstmode”-Micromachining of Metals* (Lasers in Manufacturing Congress, Munich, 2015)
25. R. Kelly, R.W. Dreyfus, Reconsidering the mechanisms of laser sputtering with Knudsen-layer formation taken into account. *Nucl. Instrum. Methods Phys. Res.* **B32**, 341–348 (1988). doi:[10.1016/0168-583X\(88\)90235-2](https://doi.org/10.1016/0168-583X(88)90235-2)
26. C.R. Phipps, R.W. Dreyfus, The high laser irradiance regime, in *Laser Ionization Mass Analysis*, ed. by A. Vertes, R. Gijbels, F. Adams (Wiley, New York, 1993), pp. 369–431
27. L. Grad, J. Mozina, Laser pulse shape influence on optically induced dynamic processes. *Appl. Surf. Sci.* (1998). doi:[10.1016/S0169-4332\(97\)00781-2](https://doi.org/10.1016/S0169-4332(97)00781-2)
28. S. Çelen, Morphological and Mechanical Analysis of Titanium Implant Surface Induced by Laser Surface Structuring. (The Graduate School of Natural and Applied Sciences Institute). Izmir, Turkey: Ege University; 2011 (Ph.D. Thesis) (2011)
29. S. Çelen, H. Ozden, Laser-induced novel patterns: as smart strain actuators for new-age dental implant surfaces. *Appl. Surf. Sci.* **263**, 579–585 (2012). doi:[10.1016/j.apsusc.2012.09.112](https://doi.org/10.1016/j.apsusc.2012.09.112)
30. S. Çelen, *Pulsed Laser-Induced Lotus Leafs from the Viewpoint of Coalescence of Sensors Hypothesis*, 18th International Conference on Surface Modification of Materials by Ion Beams, Kusadası, Turkey (2013)
31. S. Çelen, A novel strain energy density algorithm for laser-induced micro-hollows. *Opt. Lasers Eng.* (2015). doi:[10.1016/j.optlaseng.2015.02.002](https://doi.org/10.1016/j.optlaseng.2015.02.002)
32. S. Çelen, *Novel Method to Shorten the Lead Time for Laser Micro-Machining, Materials Testing*, 57th edn. (Carl Hanser Verlag GmbH & Co. KG, Berlin, 2015), pp. 585–588. doi:[10.3139/120.110751](https://doi.org/10.3139/120.110751)
33. E. Kannatey-Asibu, *Principles of Laser Materials Processing* (Wiley, Hoboken, 2009)
34. C.J. Knight, Theoretical modeling of rapid surface vaporization with back pressure. *AIAA J.* **17**, 519–523 (1979). doi:[10.2514/3.61164](https://doi.org/10.2514/3.61164)
35. A. Luft, U. Franz, A. Emsermann, J. Kaspar, A study of thermal and mechanical effects on materials induced by pulsed laser drilling. *Appl. Phys. A* **63**, 93–101 (1996). doi:[10.1007/BF01567635](https://doi.org/10.1007/BF01567635)
36. L. Grad, J. Mozina, Laser pulse shape influence on optically induced dynamic processes. *Appl. Surf. Sci.* **127**, 999–1004 (1998). doi:[10.1016/S0169-4332\(97\)00781-2](https://doi.org/10.1016/S0169-4332(97)00781-2)
37. R. Kelly, R.W. Dreyfus, On the effect of Knudsen-layer formation on studies of vaporization, sputtering and desorption. *Surf. Sci.* **198**, 263–276 (1988). doi:[10.1016/0039-6028\(88\)90483-9](https://doi.org/10.1016/0039-6028(88)90483-9)
38. S. Çelen, in preparation